Applied Mathematical Modelling 41 (2017) 462–473

Contents lists available at ScienceDirect

Applied Mathematical Modelling

journal homepage: www.elsevier.com/locate/apm

Analysis of surface mechanical properties effects on the dynamic characteristics of a circular micro-diaphragm with a distributed mass

Shasha Zhou[a], Shenjie Zhou[a,*], Binglei Wang[b], Anqing Li[a]

[a] School of Mechanical Engineering, Shandong University, Jingshi Road 17923#, Jinan 250061, China
[b] School of Civil Engineering, Shandong University, Jingshi Road 17923#, Jinan 250061, China

ARTICLE INFO

Article history:
Received 14 August 2015
Revised 22 July 2016
Accepted 14 September 2016
Available online 21 September 2016

Keywords:
Micro-diaphragm
Surface mechanical properties
Distributed mass
Dynamic characteristic

ABSTRACT

The influences of surface mechanical properties effects on the dynamic characteristics of a circular micro-diaphragm with a partially uniformly distributed mass are investigated. Surface mechanical properties effects on two sides are considered to be different as one side of the diaphragm contacts with biochemical media. A size-dependent analytical model is developed based on the thin plate theory and surface elasticity theory for the micro-diaphragm with a partially uniformly distributed mass. The Galerkin procedure is used to solve the governing equation. The size-dependence of the natural frequency and mass sensitivity of the micro-diaphragm with different surface mechanical properties effects is discussed. Results show that the influences of different surface mechanical properties effects on the natural frequency and mass sensitivity are more significant for thinner micro-diaphragms. The influences depend on the differences in the surface mechanical properties effects of the two surfaces.

1. Introduction

Resonant micro-biochemical sensors play important roles in a wide range of emerging applications to detect biochemical molecules, such as environment monitoring and medical home care [1–4]. As the resonators of micro-biochemical sensors, micro-diaphragms are used to detect biological targets by measuring the shift of the natural frequencies [5–7]. The dynamic characteristics of micro-diaphragms can be influenced by multiple effects including coupling effects of media, changing in surface mechanical properties induced by biochemical media, mass loading of adsorbates and surface effects for micro-components. The influences of one or more effects on the dynamic characteristics of macro/micro diaphragms are investigated by many researchers.

The coupling vibration of an elastic plate contacting with water on one side was studied by Lamb [8], in which the assumed mode shapes approach was used and only two mode shapes were adopted. Considering all mode shapes, Amabili and Kwak [9] revised Lamb's model to analyze the free vibration of circular plates in contact with water. Wu et al. [10] extended Lamb's fluid-solid coupled model in analyzing the effects of a distributed mass on dynamic characteristics of rectangular plates in fluid.

* Corresponding author. Fax: +86 531 88396708.
E-mail address: zhousj@sdu.edu.cn (S. Zhou).

http://dx.doi.org/10.1016/j.apm.2016.09.016
0307-904X/

The free vibration of a simply supported rectangular plate with a uniformly distributed mass in different locations was analyzed by Kopmaz and Telli [11]. Wong [12] analyzed the effects of the size and location of a distributed mass on the frequencies and mode shapes of a simply supported rectangular plate. The forced vibration of viscoelastically supported plates with a distributed mass was also be studied by many researchers [13–15]. These studies were performed for macro-plates.

For micro-plates, surface effects are prominent due to the increasing surface-to-bulk ratio [16]. To research the influence of surface effects on the free vibration of micro-plates, Lim and He [17] developed a thin plate theory based on the surface elasticity theory [18,19]. In this theory, the surface equilibrium relations could not be satisfied because of neglecting the normal stress along the surface of the bulk. Lu et al. [16] modified this model by introducing a linear normal stress in studying the size-dependent static and dynamic analysis of micro-plates. The modified model was applied to FGM plates with different surface properties by Lü et al. [20,21]. The influence of surface stresses on the vibration of circular nano-plates under various boundary conditions was analyzed applying the surface elasticity theory by Ansari et al. [22]. Using the same theory, a size-dependent analytical model for the forced vibration of rectangular nano-plates were developed [23]. Some other models based on this theory was proposed in analyzing the influence of surface effects on the deformation and vibration of nano-plates [24,25]. The shear deformation and rotational inertia were taken into account in studying the size-dependent vibration behaviors of nano-plates by Ansari and Sahmani [26] based on the surface elasticity theory. Assadi and Farshi [27] developed a size-dependent model for circular nano-plates by applying the modified laminated plate theory in studying the influence of surface effects on vibration behaviors. In above studies, the combined influences of surface effects and distributed mass, especially the different surface effects, on the dynamic characteristics of micro-components remain insufficiently investigated.

The purpose of this study is to develop an analytical model including different surface mechanical properties on two surfaces of a micro-diaphragm with a partially uniformly distributed mass. The governing equation is derived in Section 2 based on the thin plate theory and surface elasticity theory. In Section 3, the Galerkin method is introduced to solve the dynamic problem of the micro-diaphragm with surface mechanical properties effects and a distributed mass, and the approximate solution is obtained. The numerical results for natural frequency and mass sensitivity are presented in Section 4. The results of the new model are compared with the results of existing models. The size-dependent natural frequency and mass sensitivity of a circular micro-diaphragm with different material properties on top and bottom surfaces are discussed, respectively. The influence of the region of distributed mass on mass sensitivity is also discussed. Finally some concluding remarks are summarized in Section 5.

2. Equations of motion

A circular micro-diaphragm with radius a and thickness h is considered here. The elasticity modulus, Poisson's ratio, and mass density of the bulk material of the micro-diaphragm are E, ν and ρ, respectively. Surface elasticity modulus E_0^+, E_0^- are used to model the surface mechanical properties effects of top and bottom surfaces. For simplicity, the residual surface stress τ_0, Poisson's ratio $\nu_0$and density ρ_0 of the top and bottom surfaces are considered to have the same value. The partially uniformly distributed mass m_d with a radius of r_0 is considered to represent the adsorbates, which is located in the centre of the top surface, as shown in Fig. 1.

A dynamic equation including different surface mechanical properties on the top and bottom surfaces of a micro-diaphragm with a partially uniformly distributed mass can be developed based on Kirchhoff's plate theory. Considering the middle plane deformation induced by the same residual surface stress of the top and bottom surfaces, the displacement components including the elongation or compression of the middle plane are adopted.

$$u_\alpha = u_\alpha^0 - z u_{3,\alpha}, \quad u_3 = w(r,\theta,t), \tag{1}$$

where u_α are the displacement components, u_α^0 are the middle plane displacements induced by the residual surface stress and $w(r, \theta, t)$ is the deflection of the middle plane in the plate along z-axis. In Eq. (1) and followings, the Greek subscripts represent 1 and 2, while the Latin subscripts represent 1, 2 and 3. The corresponding non-zero strain components are given by

$$\varepsilon_{\alpha\beta} = \varepsilon_{\alpha\beta}^0 - z u_{3,\alpha\beta}, \quad \varepsilon_{\alpha\beta}^0 = \frac{1}{2}(u_{\alpha,\beta}^0 + u_{\beta,\alpha}^0), \tag{2}$$

As surface mechanical properties effects are considered, the constitutive relations of the bulk and surface materials are different. For isotropic materials, the constitutive relations of the bulk are expressed as

$$\sigma_{ij} = \lambda(\varepsilon_{kk}^0 - z u_{3,kk})\delta_{ij} + 2\mu(\varepsilon_{ij}^0 - z u_{3,ij}), \tag{3}$$

where σ_{ij} are the stress components, λ and μ are the Lame's constants of the bulk material and δ_{ij} is the Kronecker delta. The constitutive relations of the surface are given by [18,19,28]

$$\sigma_{\alpha\beta}^+ = \tau_0\delta_{\alpha\beta} + (\mu_0^+ - \tau_0)(u_{\alpha,\beta}^+ + u_{\beta,\alpha}^+) + (\lambda_0^+ + \tau_0)u_{\gamma,\gamma}^+\delta_{\alpha\beta} + \tau_0 u_{\alpha,\beta}^+, \quad \sigma_{\alpha3}^+ = \tau_0 u_{3,\alpha}^+, \tag{4}$$

$$\sigma_{\alpha\beta}^- = \tau_0\delta_{\alpha\beta} + (\mu_0^- - \tau_0)(u_{\alpha,\beta}^- + u_{\beta,\alpha}^-) + (\lambda_0^- + \tau_0)u_{\gamma,\gamma}^-\delta_{\alpha\beta} + \tau_0 u_{\alpha,\beta}^-, \quad \sigma_{\alpha3}^- = \tau_0 u_{3,\alpha}^-, \tag{5}$$

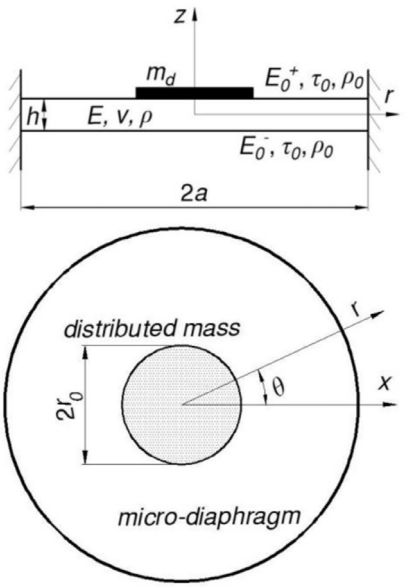

Fig. 1. Circular micro-diaphragm with surface mechanical properties and a partially uniformly distributed mass.

where μ_0 and λ_0 are surface Lame's constants, the superscripts '+' and '−' denote the stresses and displacements on the top and bottom surfaces, respectively.

The equilibrium relations for the body of the micro-diaphragm without body forces are given by

$$\sigma_{ij,j} = \rho \ddot{u}_i. \tag{6}$$

The equilibrium equations of surfaces are different from those of the body because of surface mechanical properties effects [18,28].

$$\sigma^+_{i\beta,\beta} - \sigma^+_{i3} = \rho_0 \ddot{u}^+_i \quad \text{at } z = h/2. \tag{7}$$

$$\sigma^-_{i\beta,\beta} + \sigma^-_{i3} = \rho_0 \ddot{u}^-_i \quad \text{at } z = -h/2. \tag{8}$$

The surface equilibrium Eqs. (7) and (8) will not be satisfied for the thin plate theory, because the normal stress is assumed to be zero. To modify this problem, the normal stress σ_{33} is assumed to be [16]

$$\sigma_{33} = \frac{1}{2}(\sigma^+_{3\beta,\beta} - \sigma^-_{3\beta,\beta} - \rho_0 \ddot{u}^+_3 + \rho_0 \ddot{u}^-_3) + \frac{1}{h}(\sigma^+_{3\beta,\beta} + \sigma^-_{3\beta,\beta} - \rho_0 \ddot{u}^+_3 - \rho_0 \ddot{u}^-_3)z. \tag{9}$$

Considering the normal stress, the bulk constitutive relations can be simplified as

$$\sigma_{i\beta} = \frac{E}{1+\nu}[(\varepsilon^0_{i\beta} - z u_{3,i\beta}) + \frac{\nu}{1-\nu}(\varepsilon^0_{\alpha\alpha} - z u_{3,\alpha\alpha})\delta_{i\beta}] + \frac{\nu}{1-\nu}\sigma_{33}\delta_{i\beta}. \tag{10}$$

By multiplying the body equilibrium relation Eq. (6) by dz and zdz, respectively, and integrating on the thickness, the equilibrium equations expressed by the resultant forces and moments can be obtained.

$$Q_{i\alpha,\alpha} + \sigma^+_{i3} - \sigma^-_{i3} = \int_{-h/2}^{h/2} \rho \ddot{u}_i dz, \tag{11}$$

$$M_{i\alpha,\alpha} - \int_{-h/2}^{h/2} \sigma_{i3} dz + \frac{h}{2}(\sigma^+_{i3} - \sigma^-_{i3}) = \int_{-h/2}^{h/2} \rho \ddot{u}_i z dz, \tag{12}$$

in which $Q_{i\alpha} = \int_{-h/2}^{h/2} \sigma_{i\alpha} dz$ are the resultant forces and $M_{i\alpha} = \int_{-h/2}^{h/2} \sigma_{i\alpha} z dz$ are the resultant moments. For simplicity, the generalized resultant forces $Q^*_{i\alpha}$ and resultant moments $M^*_{i\alpha}$ are introduced in the following form [16].

$$Q^*_{i\alpha} = Q_{i\alpha} + \sigma^+_{i\alpha} + \sigma^-_{i\alpha}, \tag{13}$$

$$M^*_{\alpha\beta} = M_{\alpha\beta} + \frac{h}{2}(\sigma^+_{\alpha\beta} - \sigma^-_{\alpha\beta}). \tag{14}$$

With the help of surface equilibrium Eqs. (7) and (8), the equilibrium Eqs. (11) and (12) for the resultant forces and moments can be expressed by the generalized resultant forces and moments.

$$Q^*_{i\alpha,\alpha} = \int_{-h/2}^{h/2} \rho \ddot{u}_i dz + \rho_0(\ddot{u}_i^+ + \ddot{u}_i^-), \tag{15}$$

$$M^*_{\alpha\beta,\beta} - Q^*_{3\alpha} + \sigma^+_{3\alpha} + \sigma^-_{3\alpha} = \int_{-h/2}^{h/2} \rho \ddot{u}_\alpha z dz + \frac{h}{2}\rho_0(\ddot{u}_\alpha^+ - \ddot{u}_\alpha^-). \tag{16}$$

By using the constitutive relations of the surface and bulk, the resultant forces $Q_{\alpha\beta}$ and resultant moments $M_{\alpha\beta}$ can be obtained, then the generalized resultant forces $Q^*_{\alpha\beta}$ and resultant moments $M^*_{\alpha\beta}$ are expressed as

$$Q^*_{\alpha\beta} = 2\tau_0(\delta_{\alpha\beta} + u^0_{\alpha,\beta}) + \left[\frac{Eh}{1+\nu} + 2(\mu_0^+ + \mu_0^- - 2\tau_0)\right]\varepsilon^0_{\alpha\beta} + \left[\frac{Eh\nu}{1-\nu^2} + (\lambda_0^+ + \lambda_0^- + 2\tau_0)\right]\varepsilon^0_{\alpha\alpha}\delta_{\alpha\beta}, \tag{17}$$

$$M^*_{\alpha\beta} = -\left[\frac{Eh^3}{12(1+\nu)} + \frac{(\mu_0^+ + \mu_0^-)h^2}{4}\right]u_{3,\alpha\beta} - \left[\frac{(\lambda_0^+ + \lambda_0^-)}{4} + \frac{\tau_0(3-4\nu)}{6(1-\nu)}\right]h^2 u_{3,\gamma\gamma}\delta_{\alpha\beta} - \frac{h^2\nu}{6(1-\nu)}\rho_0\ddot{u}_3\delta_{\alpha\beta}. \tag{18}$$

Substituting Eqs. (17) and (18) into the equilibrium Eqs. (15) and (16), the equations can be expressed by displacements as

$$\left[\frac{Eh}{2(1+\nu)} + (\mu_0^+ + \mu_0^- - 2\tau_0)\right](u^0_{\alpha,\beta\beta} + u^0_{\beta,\alpha\beta}) + \left[\frac{Eh\nu}{(1-\nu^2)} + (\lambda_0^+ + \lambda_0^- + 2\tau_0)\right]u^0_{\alpha,\alpha\beta}\delta_{\alpha\beta},$$
$$+2\tau_0 u^0_{\alpha,\beta\beta} = (\rho h + 2\rho_0)\ddot{u}^0_\alpha, \tag{19}$$

$$-\left[\frac{Eh^3}{12(1+\nu)} + \frac{(\mu_0^+ + \mu_0^-)h^2}{4}\right]u_{3,\alpha\beta\alpha\beta} - \left[\frac{(\lambda_0^+ + \lambda_0^-)}{4} + \frac{\tau_0(3-4\nu)}{6(1-\nu)}\right]h^2 u_{3,\gamma\gamma\alpha\beta}\delta_{\alpha\beta} + 2\tau_0 u_{3,\alpha\alpha}.$$
$$= (\rho h + 2\rho_0)\ddot{u}_3 - \left[\frac{\rho h^3}{12} + \frac{(3-4\nu)\rho_0 h^2}{6(1-\nu)}\right]\ddot{u}_{3,\alpha\alpha} \tag{20}$$

The middle plane elongation or compression u^0_α induced by the residual surface stress τ_0 can be obtained by solving Eqs. (19), and (20) is the transverse dynamic equation including surface mechanical properties effects. If the top and bottom surfaces have the same material parameters, the equilibrium Eqs. (19) and (20) will reduce to the model without external forces and moments given by Lu et al. [16]. It can be seen that Eqs. (19) and (20) are uncoupled, that is, the initial deformation induced by the residual surface stress has no effect on the transverse vibration. For a micro-diaphragm with a partially uniformly distributed mass, the effect of the mass can be equivalent to a transverse inertia force. Thus, by introducing the transverse inertia force into Eq. (20), the governing equation that includes the partially uniformly distributed mass in the form of deflection for micro-diaphragms can be obtained.

$$D^*\nabla^4 w - 2\tau_0\nabla^2 w + \left[\rho h + 2\rho_0 + \frac{m_d}{\pi r_0^2}H(\xi,\xi_0)\right]\frac{\partial^2 w}{\partial t^2} - \left[\frac{\rho h^3}{12} + \frac{(3-4\nu)\rho_0 h^2}{6(1-\nu)}\right]\nabla^2\ddot{w} = 0, \tag{21}$$

where $H(\xi,\xi_0)$ is the Heaviside function used to define the region of the distributed mass

$$H(\xi,\xi_0) = \begin{cases} 0 \xi > \xi_0 \\ 1 \xi \le \xi_0 \end{cases}, \tag{22}$$

the non-dimensional parameters ξ and ξ_0 are defined as

$$\xi = \frac{r}{a}, \xi_0 = \frac{r_0}{a} \quad (0 \le \xi_0 \le 1, 0 \le \xi \le 1), \tag{23}$$

the symbols ∇^4 and ∇^2 are the biharmonic operator and Laplace operator in non-dimensional polar coordinates. D^* is the effective flexural rigidity including surface mechanical properties effects

$$D^* = D + \frac{h^2}{4}(\mu_0^+ + \mu_0^-) + \frac{h^2}{4}(\lambda_0^+ + \lambda_0^-) - \frac{h^2}{6}\frac{(3-4\nu)\tau_0}{(1-\nu)}, \tag{24}$$

where $D = Eh^3/12(1-\nu^2)$ is the flexural rigidity in classical continuum plate theory.

The governing Eq. (21) describes the influences of the partially uniformly distributed mass and different surface mechanical properties on the dynamic characteristics of the micro-diaphragm. When the distributed mass m_d is equal to zero and the top and bottom surfaces have the same material properties, the present model will reduce to the model without external forces and moments developed by Lu et al. [16]. While the distributed mass m_d and surface material parameters E_0, ν_0 and ρ_0 are equal to zero, the present model will reduce to the classical plate model [29]. The present model can be used to analyze the dynamic characteristics of circular micro-diaphragms with different surface mechanical properties on top and bottom surfaces and a distributed mass.

3. Approximate solution

A clamped micro-diaphragm is considered here. The boundary conditions are as follows

$$W(1,\theta)=\left.\frac{\partial W}{\partial \xi}\right|_{\xi=1}=0. \tag{25}$$

The solution of Eq. (21) can be expressed by summing a series of eigenfunctions for each separated mode as follows

$$w(\xi,\theta,t)=\sum_{m=0}^{N_m}\sum_{n=0}^{N_n}W_{mn}(\xi,\theta)q_{mn}(t), \tag{26}$$

where $q_{mn}(t)$ are the functions of time t. The modal functions W_{mn} for a clamped circular plate are taken as [30]

$$W_{mn}(\xi,\theta)=\alpha[J_m(\lambda_{mn}\xi)-\frac{1}{2}\lambda_{mn}\xi^m(1-\xi^2)J_{m+1}(\lambda_{mn})]\cos m\theta, \tag{27}$$

in which λ_{mn} are the n-th positive roots of the Bessel function $J_m(x)$ and α is

$$\alpha=\begin{cases}1 & m\neq 0\\ 1/2 & m=0\end{cases}. \tag{28}$$

By substituting Eq. (27) into Eq. (21), the governing equation can be obtained as

$$\begin{aligned}&\frac{D^*}{a^4}\sum_{m=0}^{N_m}\sum_{n=1}^{N_n}q_{mn}(\lambda_{mn})^4J_m(\lambda_{mn}\xi)\cos m\theta\\&+\frac{2\tau_0}{a^2}\sum_{m=0}^{N_m}\sum_{n=1}^{N_n}q_{mn}[(\lambda_{mn})^2J_m(\lambda_{mn}\xi)-2\lambda_{mn}\xi^m(1+m)J_{m+1}(\lambda_{mn})]\cos m\theta\\&-(\rho h+2\rho_0)\omega^2\sum_{m=0}^{N_m}\sum_{n=1}^{N_n}q_{mn}\left[J_m(\lambda_{mn}\xi)-\frac{1}{2}\lambda_{mn}\xi^m(1-\xi^2)J_{m+1}(\lambda_{mn})\right]\cos m\theta\\&-\frac{m_d}{\pi {r_0}^2}\omega^2H\sum_{m=0}^{N_m}\sum_{n=1}^{N_n}q_{mn}\left[J_m(\lambda_{mn}\xi)-\frac{1}{2}\lambda_{mn}\xi^m(1-\xi^2)J_{m+1}(\lambda_{mn})\right]\cos m\theta\\&+\frac{\omega^2}{a^2}\left[\frac{\rho h^3}{12}+\frac{(3-4\nu)\rho_0h^2}{6(1-\nu)}\right]\sum_{m=0}^{N_m}\sum_{n=1}^{N_n}q_{mn}[(\lambda_{mn})^2J_m(\lambda_{mn}\xi)-2\lambda_{mn}\xi^m(1+m)J_{m+1}(\lambda_{mn})]\cos m\theta=0.\end{aligned} \tag{29}$$

The analytical solution of the governing Eq. (29) can not be obtained. The Galerkin procedure is used to obtain the approximate solution. The weight functions are selected in the following form [30].

$$W_{m_0n_0}(\xi,\theta)=\xi J_{m_0}(\lambda_{m_0n_0}\xi)\cos m_0\theta,\quad m_0=0,1,2,...,N_m;\ n_0=0,1,2,...,N_n. \tag{30}$$

By multiplying each term by the weight functions, integrating the equation over the domain (0, 1), (0, 2π) and using the orthogonality of trigonometric functions and Bessel functions, Eq. (29) can be rewritten as

$$\begin{aligned}&C_1(m_0,n_0)q_{m_0n_0}+C_2(m_0,n_0)q_{m_0n_0}-\sum_{n=0}^{N_n}C_3(m_0,n_0,n)q_{mn}-\omega^2\rho hC_4(m_0,n_0)q_{m_0n_0}\\&+\omega^2\rho h\sum_{n=0}^{N_n}C_5(m_0,n_0,n)q_{mn}-\frac{m_d\omega^2}{\pi {r_0}^2}C_6(m_0,n_0)q_{m_0n_0}+\frac{m_d\omega^2}{\pi {r_0}^2}\sum_{n=0}^{N_n}C_7(m_0,n_0,n)q_{mn},\\&+\omega^2C_8(m_0,n_0)q_{m_0n_0}-\omega^2\sum_{n=0}^{N_n}C_9(m_0,n_0,n)q_{mn}=0\end{aligned} \tag{31}$$

in which the coefficients C_p ($p=1, 2, 3..., 9$) is presented in Appendix.

To reduce the indices in Eq. (31), indices i, j and N are taken as

$$\begin{aligned}&i=N_mm_0+n_0,\quad (m_0=0,1,2,...,N_m,n_0=0,1,2,...,N_n)\\&j=N_nm+n,\quad (m=0,1,2,...,N_m,n=0,1,2,...,N_n).\\&N=N_mN_n\qquad (i,j=0,1,2,...,N)\end{aligned} \tag{32}$$

Therefore, Eq. (31) can be simplified as

$$[C_1(i)+C_2(i)]q_i-\sum_{j=1}^{N}C_3(i,j)q_j-\omega^2 q_i[\rho hC_4(i)+\frac{m_d}{\pi {r_0}^2}C_6(i)-C_8(i)].$$

$$+\omega^2 q_j[\rho h\sum_{j=1}^{N}C_5(i,j)+\frac{m_d}{\pi {r_0}^2}\sum_{j=1}^{N}C_7(i,j)-\sum_{n=0}^{N_n}C_9(i,j)]=0 \tag{33}$$

Further, Eq. (33) can be expressed in matrix form as follows

$$\{\omega^2[[\mathbf{Q}]-[\mathbf{I}]+[\mathbf{M}]]\}\{\mathbf{q}\}=\{0\}, \tag{34}$$

where [**I**] is the unit matrix, [**M**] is the diagonal matrix and [**Q**] is the $N\times N$ square matrix. The elements M_i and $Q_{ij}$of matrix [**M**] and matrix [**Q**] are

$$M_i=\frac{C_1(i)+C_2(i)-C_3(i,j)}{[\rho hC_4(i)+\frac{m_d}{\pi {r_0}^2}C_6(i)-C_8(i)]}, \tag{36}$$

and

$$Q_{ij}=\frac{[\rho hC_5(i,j)+\frac{m_d}{\pi {r_0}^2}C_7(i,j)-C_9(i,j)]}{[\rho hC_4(i)+\frac{m_d}{\pi {r_0}^2}C_6(i)-C_8(i)]}. \tag{37}$$

For the non-trivial solutions of {**q**} in Eq. (35), the determinant of the coefficients matrix must be zero. The explicit form of this characteristic determinant can be expressed as follow

$$\begin{vmatrix} (Q_{11}-1)\omega^2+M_1 & Q_{12}\omega^2 & Q_{13}\omega^2 & \dots & Q_{1N}\omega^2 \\ Q_{21}\omega^2 & (Q_{22}-1)\omega^2+M_2 & Q_{23}\omega^2 & \dots & Q_{2N}\omega^2 \\ \vdots & & & & \\ \vdots & & & & \\ Q_{N1}\omega^2 & Q_{N2}\omega^2 & Q_{N3}\omega^2 & \dots & (Q_{NN}-1)\omega^2+M_N \end{vmatrix}=0. \tag{38}$$

The natural frequency of the micro-diaphragm with surface mechanical properties effects and a partially uniformly distributed mass can be obtained by solving the characteristic equation.

4. Numerical results and discussions

The numerical results of Eq. (38) become more accurate with the increase of N. The numerical result of a circular plate with free boundary conditions is sufficiently accurate when $N_n= N_m=10$ [30]. Thus, the values $N_m=10$, $N_n=10$, $N=N_mN_n=100$ are adopted.

4.1. Size dependence of natural frequency

Firstly, to evaluate the validity, the reduced model of present study, in which the distributed mass is equal to zero and two surfaces have the same surface properties, is compared with the model of Assadi and Farshi [27]. The material parameters and geometric dimension are the same as those of Assadi and Farshi [27]. A comparison is shown in Fig. 2, where ω_s and ω_0 are the natural frequencies of micro-diaphragms with and without surface mechanical properties effects, respectively. It can be seen that the two models predict the same tendency of size-dependent natural frequency. In other words, the size-dependence of natural frequency can be predicted by both the present model and the model of Assadi and Farshi [27]. However, the result of the reduced model is a little smaller than that of modified laminated plate theory, because the influence of residual surface stress on the effective flexural rigidity is not introduced in the modified laminated plate theory. This results in a larger effective flexural rigidity of the model of Assadi and Farshi [27] than the reduced model. Therefore, the results of the reduced model are smaller.

In what follows, the influence of surface mechanical properties on the first order natural frequency and mass sensitivity of the micro-diaphragm is analyzed. The diaphragm made of silicon is considered as the example. For silicon ($E=210\times10^9$N/m^2, $E_0=-10.036$N/m and $\rho=2331$ kg/m^3), the residual surface stress and surface density are given as $\tau_0=0.605$N/m and $\rho_0=3.17\times10^{-7}$kg/m^2 [31]. The radius of the circular micro-diaphragm is taken as $a=4\times10^{-4}$m [32]. The Poisson's ratio v_0 of the surface layers material is taken to be equal to that of the bulk material: $v_0=v=0.24$ [27,33,34].

For the top and bottom surfaces with the same surface mechanical properties, the natural frequencies of the micro-diaphragm with the varying thickness for different E_0 are shown in Fig. 3. Compared with the results of classical plate model without surface effects [29], for both the stiffened ($E_0 > 0$) and softened ($E_0 < 0$) surfaces, if the thickness h is smaller than about $1\times10^{-8}m$, the natural frequencies have stronger size-dependence. The natural frequencies increase with the decrease of thickness for the stiffened surfaces. While for the softened surfaces, the natural frequencies decrease with the decrease of thickness. Moreover, the stiffened surface can increase the natural frequency, and the influence is more

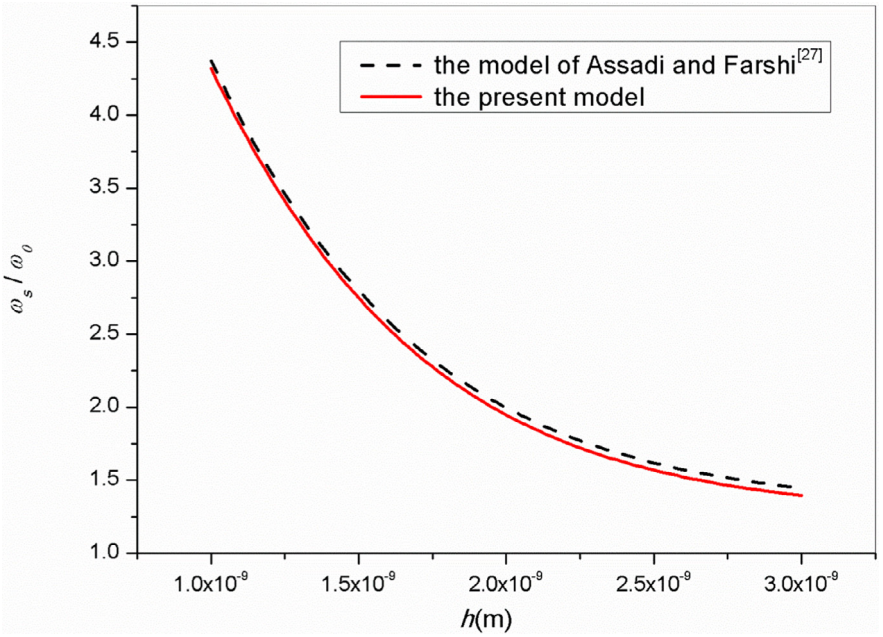

Fig. 2. Size-dependent natural frequency of the micro-diaphragm ($m=1$, $n=1$).

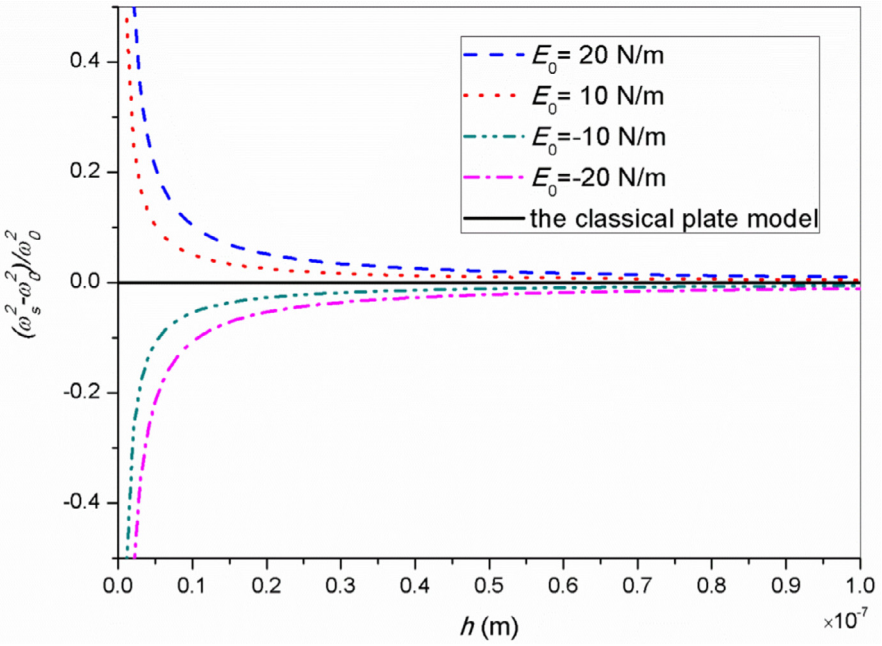

Fig. 3. Size-dependent natural frequency of the micro-diaphragm for the case of top and bottom surfaces with the same surface mechanical properties ($m_d=0$ kg).

significant for largerE_0. The softened surface can decrease the natural frequency, and the influence is more significant for smaller E_0.

Different surface mechanical properties on two sides are considered as the top surface of the micro-diaphragm contacts with biochemical media. For the top and bottom surfaces with different surface mechanical properties, the natural frequencies of the micro-diaphragm with the varying thickness for different ΔE_0 are shown in Fig. 4, where the difference in surface elasticity modulus $\Delta E_0 = E_0^+ - E_0^-$ is defined. As seen in Fig. 4, the direction of the variation depends on the sign of ΔE_0. The natural frequencies increase for $\Delta E_0 > 0$, and increase with the decrease of thickness. While for $\Delta E_0 < 0$, the natural

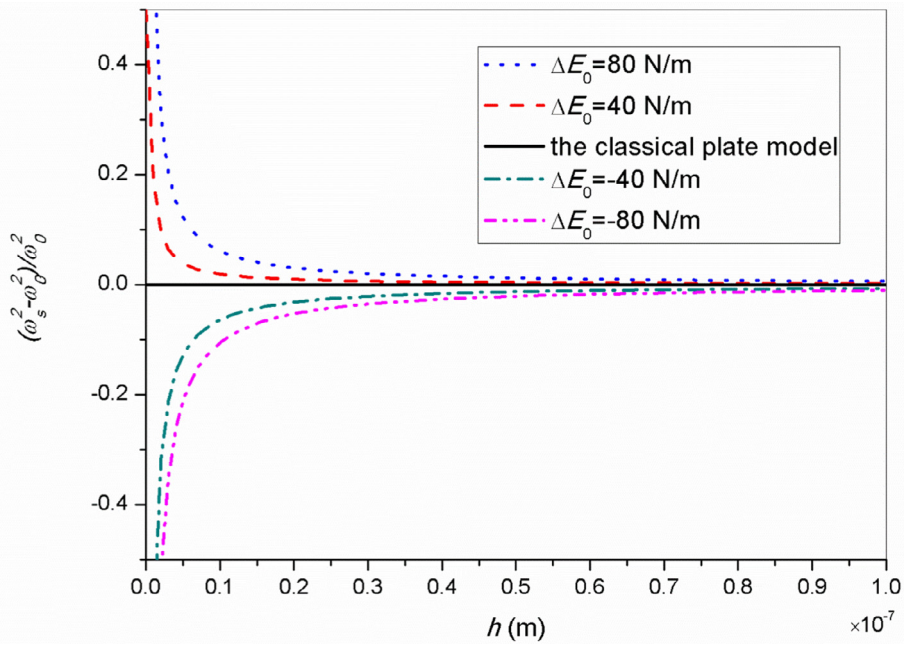

Fig. 4. Size-dependent natural frequency of the micro-diaphragm for the case of top and bottom surfaces with different surface mechanical properties ($m_d = 0$kg).

frequencies decrease with the decrease of thickness. In addition, the natural frequencies increase with the increase of ΔE_0 for both the stiffened and softened surfaces.

4.2. Size dependence of mass sensitivity

Mass sensitivity is an important performance index of resonant micro-biochemical sensors. Considering surface mechanical properties effects, the mass sensitivity has the following form [35].

$$S_m = \frac{\Delta\omega}{m_d}, \tag{39}$$

in which $\Delta\omega = |\omega_a - \omega_b|$ is the adsorption-induced frequency shift of the circular micro-diaphragm. ω_a and ω_b are the natural frequencies measured after and before the partially uniformly distributed mass m_d adsorbed, respectively. For the case of no surface mechanical properties effects, the mass sensitivity is denoted as S_m^0.

When the top and bottom surfaces have the same surface mechanical properties, the variations of the normalized mass sensitivity with respect to the thickness for different E_0 are shown in Fig. 5. The results predicated by the present model are compared with that of the classical plate model [29] that has no surface mechanical properties effects. For the present model, the stiffened surface can increase the mass sensitivity, while the softened surface can decrease it. For stiffened surfaces, the mass sensitivity increases with the decrease of thickness. For softened surfaces, the mass sensitivity decreases with the decrease of thickness. If the thickness h is smaller than about $1 \times 10^{-8} m$, the normalized mass sensitivity has stronger size-dependence for both the stiffened and softened surfaces; however, as the thickness increases its influence diminishes and the normalized mass sensitivity tends to get closer to results of classical plate model. It indicates that the influence of surface mechanical properties on the mass sensitivity of the micro-diaphragm is more significant in thinner micro-diaphragms for both stiffened and softened surfaces.

For the top and bottom surfaces with different surface mechanical properties, the normalized mass sensitivities of the micro-diaphragm versus thickness with different ΔE_0 are shown in Fig. 6. It can be seen that the tendencies of the size-dependent mass sensitivity in Fig. 6 are similar to the tendencies of the size-dependent natural frequency in Fig. 4. For surfaces with $\Delta E_0 > 0$, mass sensitivity increases with the decrease of thickness. For surfaces with $\Delta E_0 < 0$, mass sensitivity decreases with the decrease of thickness. Moreover, mass sensitivity increases with the increase of ΔE_0 for both $\Delta E_0 > 0$ and $\Delta E_0 < 0$. The influence of different surface mechanical properties on the mass sensitivity is also more obvious for thinner micro-diaphragms.

The influence of the non-dimensional distributed radius on the mass sensitivity for stiffened and softened surfaces is discussed in Fig. 7. Compared with the classical plate model [29] that has no surface mechanical properties effects, the surface with $\Delta E_0 > 0$ can increase the mass sensitivity while the surface with $\Delta E_0 < 0$ can decrease it. These results can

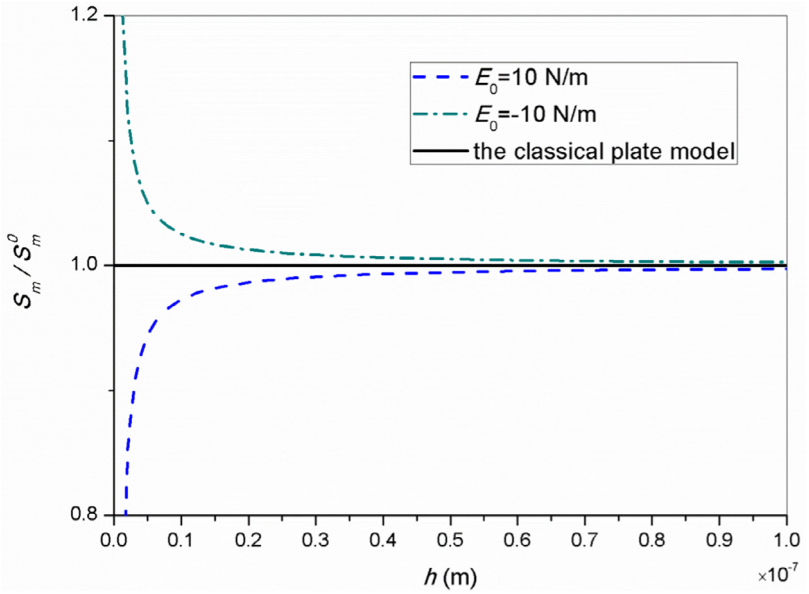

Fig. 5. Size-dependent mass sensitivity of the micro-diaphragm for the case of top and bottom surfaces with the same surface mechanical properties ($m_d = 3 \times 10^{-9}$kg, ξ_0=0.5).

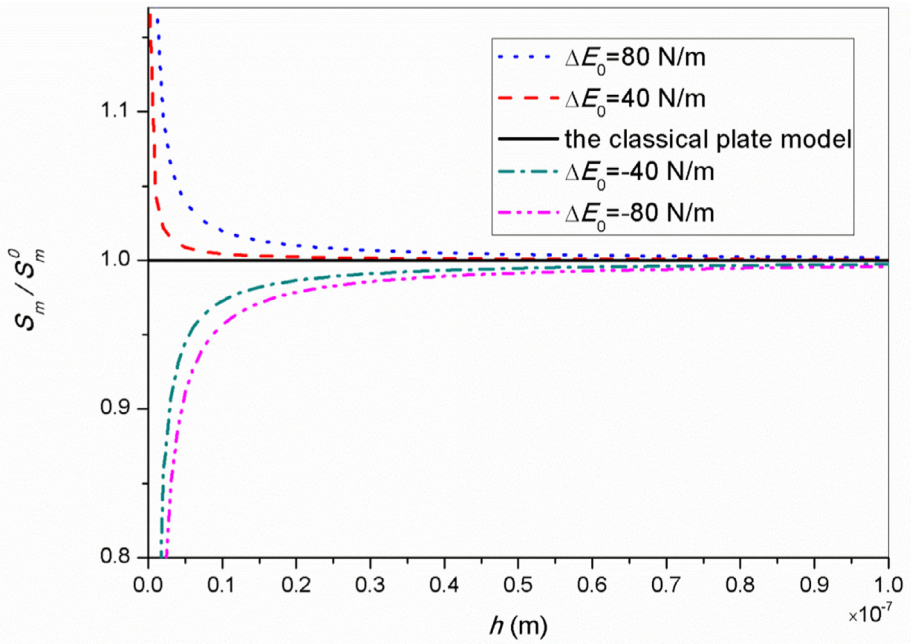

Fig. 6. Size-dependent mass sensitivity of the micro-diaphragm for the case of top and bottom surfaces with different surface mechanical properties ($m_d = 3 \times 10^{-9}$kg, ξ_0=0.5).

be also observed in Fig. 5. Moreover, for the surfaces with both $\Delta E_0 > 0$ and $\Delta E_0 < 0$, the mass sensitivity increases as the non-dimensional distributed radius decreases.

5. Conclusion

The dynamic characteristics of a circular micro-diaphragm with a partially uniformly distributed mass are analyzed together with different surface mechanical properties effects. The different surface mechanical properties effects are taken into account based on the surface elasticity theory. The approximate solution is obtained through the Galerkin procedure. The present model can reduced to the existing models. The influence of different surface mechanical properties on the natural

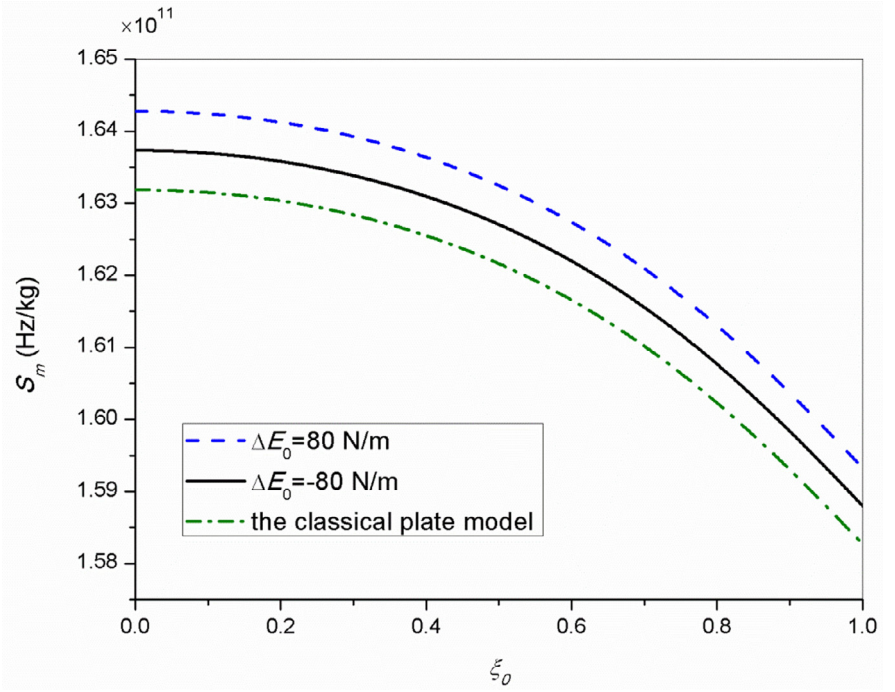

Fig. 7. Mass sensitivity varying with the non-dimensional distributed radius in the cases of stiffened and softened surfaces ($h=1\times10^{-8}$ m, $m_d=3\times10^{-9}$ kg).

frequency and mass sensitivity is discussed. The results show that compared with the classical model, the influences of the stiffened and softened surfaces on the natural frequency and mass sensitivity depend on the surface elasticity modulus E_0 and the difference in surface elasticity modulus ΔE_0. Compared with the results of two surfaces with the same surface mechanical properties, different surface mechanical properties of the top and bottom surfaces result in the different size-dependence. For both stiffened and softened surfaces, mass sensitivity increased as the non-dimensional distributed radius decreased.

Acknowledgments

This work was supported by the National Natural Science Foundation of China [11272186, 11202117], Specialized Research Fund for the Doctoral Program of Higher Education of China [20120131110045], and the Natural Science Fund of Shandong Province of China [ZR2012AM014, BS2012ZZ006].

Appendix A

The coefficients C_p ($p=1, 2, 3..., 9$) are expressed as

$$C_1(m_0,n_0)=\begin{cases}\dfrac{\pi D^*}{4a^4}(\lambda_{_0n_0})^4{J_1}^2(\lambda_{0n_0}) & m=m_0=0,n=n_0\\ \dfrac{\pi D^*}{2a^4}(\lambda_{m_0n_0})^4{J_{m_0+1}}^2(\lambda_{m_0n_0}) & m=m_0\neq0,n=n_0\end{cases}, \tag{A1}$$

$$C_2(m_0,n_0)=\begin{cases}\dfrac{\tau_0\pi}{a^2}(\lambda_{_0n_0})^2{J_1}^2(\lambda_{0n_0}) & m=m_0=0,n=n_0\\ \dfrac{\tau_0\pi}{a^2}(\lambda_{m_0n_0})^2{J_{m_0+1}}^2(\lambda_{m_0n_0}) & m=m_0\neq0,n=n_0\end{cases}, \tag{A2}$$

$$C_3(m_0,n_0,n)=\begin{cases}\dfrac{4\tau_0\pi}{a^2}\dfrac{J_1(\lambda_{0n_0})}{\lambda_{0n_0}}\lambda_{0n}J_1(\lambda_{0n}) & m=m_0=0\\ \dfrac{4\tau_0\pi}{a^2}(m_0+1)\dfrac{J_{m_0+1}(\lambda_{m_0n_0})}{\lambda_{m_0n_0}}\lambda_{m_0n}J_{m_0+1}(\lambda_{m_0n}) & m=m_0\neq0\end{cases}, \tag{A3}$$

$$C_4(m_0,n_0)=\begin{cases}\dfrac{\pi}{2}{J_1}^2(\lambda_{0n_0}) & m=m_0=0,n=n_0\\ \dfrac{\pi}{2}{J_{m_0+1}}^2(\lambda_{m_0n_0}) & m=m_0\neq 0,n=n_0\end{cases}, \tag{A4}$$

$$C_5(m_0,n_0,n)=\begin{cases}\dfrac{\pi}{2}J_1(\lambda_{0n})\lambda_{0n}\displaystyle\int_0^1\xi(1-\xi^2)J_0(\lambda_{0n_0}\xi)d\xi & m=m_0=0\\ \dfrac{2\pi(m_0+1)}{(\lambda_{m_0n_0})^3}J_{m_0+1}(\lambda_{m_0n_0})\lambda_{m_0n}J_{m_0+1}(\lambda_{m_0n}) & m=m_0\neq 0\end{cases}, \tag{A5}$$

$$C_6(m_0,n_0)=\begin{cases}\pi\displaystyle\int_0^{\xi_0}\xi{J_0}^2(\lambda_{0n_0}\xi)d\xi & m=m_0=0,n=n_0\\ \pi\displaystyle\int_0^{\xi_0}\xi{J_{m_0}}^2(\lambda_{m_0n_0}\xi)d\xi & m=m_0\neq 0,n=n_0\end{cases}, \tag{A6}$$

$$C_7(m_0,n_0,n)=\begin{cases}\dfrac{\pi}{2}(\lambda_{0n})J_1(\lambda_{0n})\left[\displaystyle\int_0^{\xi_0}\xi(1-\xi^2)J_0(\lambda_{0n_0}\xi)\right]d\xi & m=m_0=0\\ \dfrac{\pi}{2}(\lambda_{m_0n})J_{m_0+1}(\lambda_{m_0n})\left[\displaystyle\int_0^{\xi_0}\xi^{m_0+1}(1-\xi^2)J_{m_0}(\lambda_{m_0n_0}\xi)\right]d\xi & m=m_0\neq 0\end{cases}, \tag{A7}$$

$$C_8(m_0,n_0)=\begin{cases}\dfrac{\pi}{2a^2}\left[\dfrac{\rho h^3}{12}+\dfrac{\nu\rho_0h^2}{6(1-\nu)}\right](\lambda_{0n_0})^2{J_1}^2(\lambda_{0n_0}) & m=m_0=0,n=n_0\\ \dfrac{\pi}{2a^2}\left[\dfrac{\rho h^3}{12}+\dfrac{\nu\rho_0h^2}{6(1-\nu)}\right](\lambda_{m_0n_0})^2{J_{m_0+1}}^2(\lambda_{m_0n_0}) & m=m_0\neq 0,n=n_0\end{cases}, \tag{A8}$$

$$C_9(m_0,n_0,n)=\begin{cases}\dfrac{2\pi}{a^2}\left[\dfrac{\rho h^3}{12}+\dfrac{(3-4\nu)\rho_0h^2}{6(1-\nu)}\right]\dfrac{J_1(\lambda_{0n_0})}{\lambda_{0n_0}}\lambda_{0n}J_1(\lambda_{0n}) & m=m_0=0\\ \dfrac{2\pi}{a^2}\left[\dfrac{\rho h^3}{12}+\dfrac{(3-4\nu)\rho_0h^2}{6(1-\nu)}\right](m_0+1)\dfrac{J_{m_0+1}(\lambda_{m_0n_0})}{\lambda_{m_0n_0}}\lambda_{m_0n}J_{m_0+1}(\lambda_{m_0n}) & m=m_0\neq 0\end{cases}, \tag{A9}$$

References

[1] H.J. Lee, K.K. Park, M. Kupnik, N.A. Melosh, B.T. Khuri-Yakub, Mesoporous thin-film on highly-sensitive resonant chemical sensor for relative humidity and CO_2 detection, Anal. Chem. 84 (2012) 3063–3066.
[2] B. Ilic, Y. Yang, H.G. Craighead, Virus detection using nanoelectromechanical devices, Appl. Phys. Lett. 85 (2004) 2604–2606.
[3] A. Passian, P.G. Evans, V.K. Varma, T.L. Ferrell, T. Thundat, Piezoresistive detection of acoustic waves, Rev. Sci. Instrum 74 (2003) 1031–1035.
[4] D. Ramos, M. Calleja, J. Mertens, A. Zaballos, J. Tamayo, Measurement of the mass and rigidity of adsorbates on a microcantilever sensor, Sensors 7 (2007) 1834–1845.
[5] K. Eom, H.S. Park, D.S. Yoon, T. Kwon, Nanomechanical resonators and their applications in biological/chemical detection: nanomechanics principles, Phys. Rep 503 (2011) 115–163.
[6] S.Q. Li, Z.M. Li, B.B. Chin, Z.Y. Cheng, Development of biosensor based on microdiphragm, Proc. SPIE 5389 (2004) 306–313.
[7] Y. Xin, Z.M. Li, L. Odum, Z.Y. Cheng, Z. Xu, Piezoelectric diaphragm as a high performance biosensor platform, Appl. Phys. Lett. 89 (2006) 223508.
[8] H. Lamb, On the vibrations of an elastic plate in contact with water, Proc. R. Soc. Lond., Ser. A 98 (1920) 205–216.
[9] M. Amabili, M.K. Kwak, Free vibrations of circular plates coupled with liquids: revising the lamb problem, J. Fluid. Struct. 10 (1996) 743–761.
[10] Z.M. Wu, X.H. Ma, P.N. Brett, J.W. Xu, Vibration analysis of submerged rectangular microplates with distributed mass loading, Proc. R. Soc. A-Math. Phys. 465 (2009) 1323–1336.
[11] O. Kopmaz, S. Telli, Free vibrations of a rectangular plate carrying a distributed mass, J. Sound Vib. 251 (2002) 39–57.
[12] W.O. Wong, The effects of distributed mass loading on plate vibration behavior, J. Sound Vib. 252 (2002) 577–583.
[13] G. Altintas, M. Bagci, Determination of the steady-state response of viscoelastically supported rectangular specially orthotropic plates with varying supported area, Int. J. Eng. Model 17 (2004) 61–69.
[14] G. Altintas, A.B. Goktepe, The effect of orthotropic materials on the vibration characteristics of structural systems, Mech. Based Des. Struct. 35 (2007) 363–380.
[15] A. Ergut, G. Altintas, Effect of application area distributions of mass, fore, and support on free and forced vibration behavior of viscoelastically supported plates, J. Vib. Control. 19 (2013) 1386–1394.
[16] P. Lu, L.H. He, H.P. Lee, C. Lu, Thin plate theory including surface effects, Int. J. Solids. Struct. 43 (2006) 4631–4647.
[17] C.W. Lim, L.H. He, Size-dependent nonlinear response of thin elastic films with nanoscale thickness, Int. J. Mech. Sci. 46 (2004) 1715–1726.
[18] M.E. Gurtin, A.I. Murdoch, A continuum theory of elastic material surfaces, Arch. Ration. Mech. Anal. 57 (1975) 291–323.
[19] M.E. Gurtin, A.I. Murdoch, Addenda to our paper a continuum theory of elastic material surfaces, Arch. Ration. Mech. Anal. 59 (1975) 389–390.
[20] C.F. Lü, C.W. Lim, W.Q. Chen, Size-dependent elastic behavior of FGM ultra-thin films based on generalized refined theory, Int. J. Solids. Struct. 46 (2009) 1176–1185.
[21] C.F. Lü, W.Q. Chen, C.W. Lim, Elastic mechanical behavior of nano-scaled FGM films incorporating surface energies, Compos. Sci. Technol. 69 (2009) 1124–1130.
[22] R. Ansari, R. Gholami, M. Faghih Shojaei, V. Mohammadi, S. Sahmani, Surface stress effect on the vibrational response of circular nanoplates with various edge supports, J. Appl. Mech. 80 (2013) 021021.
[23] A. Assadi, Size dependent forced vibration of nanoplates with consideration of surface effects, Appl. Math. Model. 37 (2012) 3573–3588.

[24] L.H. He, C.W. Lim, B.S. Wu, A continuum model for size-dependent deformation of elastic films of nano-scale thickness, Int. J. Solids. Struct. 41 (2004) 847–857.
[25] C. Liu, R.K.N.D. Rajapakse, A size-dependent continuum model for nanoscale circular plates, IEEE Trans. Nanotechnol 12 (2013) 13–20.
[26] R. Ansari, S. Sahmani, Surface stress effects on the free vibration behavior of nanoplates, Int. J. Eng. Sci. 49 (2011) 1204–1215.
[27] A. Assadi, B. Farshi, Vibration characteristics of circular nanoplates, J. Appl. Phys. 108 (2010) 074312.
[28] M.E. Gurtin, A.I. Murdoch, Surface stress in solids, Int. J. Solids. Struct. 14 (1978) 431–440.
[29] S.P. Timoshenko, S. Woinowsky-Krieger, Theory of Plates and Shells, McGraw Hill, New York, 1959.
[30] Z.D. Yan, Solution of bending and buckling problems of circular plates by taking bessel functions as trial functions and weighting functions, Trans. Tianjin Univ 4 (1983) 115–125.
[31] Y.M. Fu, J. Zhang, Size-dependent pull-in phenomena in electrically actuated nanobeams incorporating surface energies, Appl. Math. Model. 35 (2011) 941–951.
[32] M. Olfatnia, Z. Shen, J.M. Miao, L.S. Ong, T. Xu, M. Ebrahimi, Medium damping influences on the resonant frequency and quality factor of piezoelectric circular microdiaphragm sensors, J. Miceomech. Microeng 21 (2011) 045002.
[33] G.F. Wang, X.Q. Feng, Effects of surface elasticity and residual surface tension on the natural frequency of microbeams, Appl. Phys. Lett. 90 (2007) 231904.
[34] P. Lu, H.P. Lee, C. Lu, S.J. O'Shea, Surface stress effects on the resonance properties of cantilever sensors, Phys. Rev. B 72 (2005) 085405.
[35] M.K. Ghatkesar, V. Braun, T. Braun, J.P. Ramseyer, C. Gerber, M. Hegner, H.P. Lang, U. Drechsler, M. Despont, Higher modes of vibration increase mass sensitivity in nanomechanical microcantilevers, Nanotechnology 18 (2007) 445502.